Finite-lattice expansion for the Ising model on the Penrose tiling

2002 J. Phys. A: Math. Gen. 35 7753

(http://iopscience.iop.org/0305-4470/35/36/304)

INSTITUTE OF PHYSICS PUBLISHING JOURNAL OF PHYSICS A: MATHEMATICAL AND GENERAL

J. Phys. A: Math. Gen. **35** (2002) 7753–7772 PII: S0305-4470(02)31630-5

Finite-lattice expansion for the Ising model on the Penrose tiling

Przemyslaw Repetowicz

Department of Mathematics, Heriot-Watt University, Riccarton, Edinburgh EH14 4AS, UK

Received 4 December 2001, in final form 20 May 2002
Published 28 August 2002
Online at stacks.iop.org/JPhysA/35/7753

Abstract

Low-temperature series are calculated for the free energy, magnetization, susceptibility and field derivatives of the susceptibility in the Ising model on the quasiperiodic Penrose lattice. The series are computed to an order of 25 and estimates of the critical exponents α, β and γ are obtained from Padé approximants.

PACS numbers: 05.50.+q, 61.44.Br, 64.60.−I, 64.60.Fr

1. Introduction

The problem of the relevance of disorder for phase transitions in lattice models of statistical mechanics has attracted attention for many years and the discovery of quasicrystals [1] has served to increase the interest in the physical properties of disordered systems. A fundamental problem in this field is whether quasiperiodic order is strong enough to change the critical behaviour of magnetic phase transitions. To investigate this problem we consider in this paper a classical Ising model defined on an underlying quasiperiodic lattice.

There have been many works in this field since the late 1980s (for a review article on aperiodic spin models, see [2]). A heuristic criterion (Harris–Luck criterion) has been formulated [3] which relates the critical behaviour to fluctuations of the number of spin couplings in a given region. The spatial scaling of fluctuations was described in terms of a 'wandering exponent' ω which was required to exceed a threshold ω_c in order to produce a new universality class. For the majority of quasiperiodic structures used to model real materials, ω can be calculated exactly due to the self-similarity or inflational symmetry of the structure, yielding a value smaller than the threshold and suggesting the irrelevance of disorder. However since numerous structures such as the rhombic sevenfold or ninefold lattices [4, 5] exist, which are deprived of inflational symmetry and are therefore potential candidates for novel critical behaviour, there is still a strong motivation for dealing with quasiperiodic Ising models. Moreover, it is relatively easy to produce a two-dimensional (2D) lattice which is

periodic in one direction and aperiodic (quasiperiodic) in the other and for which $\omega > \omega_c$. This results from the fact that 2D Ising models on such lattices are equivalent to 1D quantum Ising models (Ising quantum chains) and it is easy to generate aperiodic Ising quantum chains with relevant fluctuations where coupling constants are modulated according to certain substitution rules [6].

Quasiperiodic Ising models were investigated by Monte Carlo simulations [7–10] which at present, seem to yield the most precise estimates for the transition temperature and critical exponents. Indeed, in [8] computations for large periodic approximants (PAs) of the Penrose tiling (PT) [11] were carried out and obtained values for the correlation length ν and the two-spin correlation function η exponents with two-digit precision ($\nu = 1.02 \pm 0.02, \eta = 0.252 \pm 0.003$) which agreed with the square lattice values ($\nu = 1, \eta = 0.25$). Moreover, the non-universal critical temperature T_c has also been determined with an impressively small error $kT_c = 2.398 \pm 0.003$.

It is worth mentioning that a novel invaded-cluster algorithm, which modifies the temperature during the simulation towards the critical one, as opposed to standard Monte Carlo algorithms with fixed temperature, was also applied to quasiperiodic systems [10] to give an improved estimate of T_c. The critical exponents are not available in this case, however.

Another approach is an approximate renormalization group analysis [12, 13] which yields poor results, however. For the PT the specific heat exponent equals $\alpha = -0.1083$ versus $\alpha = 0$ for the square lattice.

Quasiperiodic Ising models were also examined by graphical expansion methods [14, 15] and by calculating exact partition functions for PAs, obtained from the Kac–Ward determinant [29]. In the first case, estimates for T_c and critical exponents have not been considerably improved but this approach demonstrated a new feature, a very slow convergence of the partition function (Z) series to its predicted asymptotic form. We also investigated the set of zeros of Z in the complex plane (Fisher zeros), which turned out to be much more complicated than in the square lattice case.

The Kac–Ward determinant method appeared to yield highly accurate estimates of the critical temperature of quasiperiodic Ising models (for example, $kT_c = 2.397\,820(7)$ for the PT). Moreover, within this framework it was possible to construct a $2D$ Ising model with relevant fluctuations, i.e. for which $\omega > \omega_c$, which shows up another novel feature, namely the divergence of high temperature series [17]. This example is interesting because it points out that in some cases the reliability of methods for extracting critical values from analysis of a series expansion, such as the Padé- or differential-approximants methods [16] can be questioned. An inspection of the Fisher zeros furnished the explanation, since it appeared that the moduli of some complex zeros were smaller than the modulus of the physical singularity (real zero) and thus the complex zeros, rather than the real zero, were limiting the region of convergence of the series.

In this paper it is not our purpose to improve on estimating T_c or α for quasiperiodic Ising models since, due to the slow convergence of series expansions [29], a large, inaccessible number of terms is needed to make progress in this field. Instead, we aim at generalizing the series expansion approach to the case of non-zero field quasiperiodic Ising or Potts models [18] and provide alternative estimates of the magnetic exponents, β, and γ. Moreover, there is the problem of a disorder-driven 'softening' of the first-order phase transition in the Q-state Potts model for $Q > 4$, which attracted much attention recently; it has been studied by Monte Carlo simulations on random-bond lattices [19, 21], deterministic lattices [20], quenched ensembles of random graphs [23] and by high-temperature series expansion methods on random-bond lattices [22], and which can be investigated in an alternative way within our framework.

2. The finite lattice expansion method for Ising models

The problem consists of calculating the partition function $Z(\mathcal{G})$ of an Ising model on a lattice $\mathcal{G}$ by series expansion. The partition function with field B and coupling constant J is defined in the usual way:

$$Z(\mathcal{G}) = \sum_{\{\sigma_j\}} \exp\beta \left\{ -J \sum_{\langle j,k \rangle} \Delta(\sigma_j, \sigma_k) - B \sum_{j=1}^{N} \Delta(\sigma_j, 0) \right\}$$
$$\text{where} \quad \Delta(\sigma_1, \sigma_2) = \begin{cases} 0 & \sigma_1 = \sigma_2 \\ 1 & \text{otherwise} \end{cases} \tag{1}$$

where the sum over spin configurations $\{\sigma_j\} = \{\sigma_1, \sigma_2, \ldots, \sigma_N\}$ consists of N sums each of which runs over $\sigma_j = \{1, 2\}$. Starting from cluster integral theory [24, pp 42–6, p 73] one can formulate a free energy (F) expansion in terms of connected graphs for a wide range of models from statistical mechanics. In particular, for the non-zero field Ising model or the Q-state Potts models (the generalization of the former one with Q values of spin at each site) the expansion on a lattice $\mathcal{G}$ reads

$$\log Z(\mathcal{G}) = \sum_r (C_r; \mathcal{G}) k_r(w) \qquad \text{where} \quad w = \tanh\beta J \tag{2}$$

where the sum on the right-hand side runs over connected graphs C_r from $\mathcal{G}$. The quantity $(C_r; \mathcal{G})$ denotes the embedding number of C_r in $\mathcal{G}$, counting the number of ways C_r can be embedded in $\mathcal{G}$. Finally, the weight functions $k_r(w)$ depend only on C_r, not on G. Making use of the independence of weights $k_r(w)$ from the lattice, we can write equation (2) substituting each connected graph C_r for $\mathcal{G}$, solve the system of equations for the weights and plug in the results to equation (2). We obtain

$$\log Z(\mathcal{G}) = \sum_{g_r} a_r \log Z(g_r) \tag{3}$$

where $a_r = \sum_p (g_p; G) b_{r,p}$ and $b_{r,p}$ is inverse to the matrix of embedding numbers, i.e. $b_{r,p} = (g_r; g_p)^{-1}$. The sum on the right-hand side in (3) runs over g_r from a subset of all connected graphs. It turns out [25] that the graph g_r can furnish a non-vanishing contribution, i.e. $a_r \neq 0$, if and only if it is an overlap of the embeddings of two other graphs having non-vanishing contributions. The construction of graphs therefore runs as follows: we start from several 'fairly large' graphs and construct all possible overlaps of their embeddings in the lattice in a recursive way. This limits the number of contributing graphs considerably, when compared to expansion (2), but, except for regular lattices such as the square or honeycomb lattice, still leaves the problem of determining g_r and the contributions a_r open. Indeed, for the square lattice where g_r are rectangles, a_r can be explicitly expressed via the ratio of the graph side lengths [26], and the order to which the expansion is correct is in direct connection with the perimeter length of the largest graphs under consideration. For the quasiperiodic lattices which we wish to investigate, the problem is not so simple. In what follows we focus on the PT [11] and present the details of the expansion method for it in the next section.

3. Calculation of series expansion for the Penrose tiling

The PT is an aperiodic tiling of a plane by two kinds of rhombi of unit length side with angles $2\pi/5$ and $4\pi/5$, respectively. A discussion of the methods of generation and geometrical properties of this tiling can be found in [15]; here we only mention a particularly useful

feature, namely that embedding numbers of finite patches from this tiling can be calculated exactly and take the form $n + m\tau$ where $\tau = (\sqrt{2} + 1)/2$ is the golden number and n, m are rational numbers. The calculation of the series expansion consists, therefore, of the following steps:

1. Choose an initial set of 'fairly large' graphs which are expected to be large enough that every connected subgraph of the underlying tiling with perimeter length not larger than a given threshold $2L$ can be embedded in one of them. While on the square lattice this condition is satisfied by all possible rectangles with perimeter length $2L$, on the PT things are worse due to the lack of periodicity of the tiling. Moreover, as opposed to the square lattice, graphs in the PT can have different 'boundary line fillings', i.e. there are different graphs having the same boundary line [15]. Knowing that the PT contains eight different vertex types, i.e. different site environments related to the nearest neighbours, we cut out appropriately large patches around each vertex type, obtaining eight patches, and found all possible 'boundary line fillings'. There is still a lot of ambiguity in this procedure since a patch is not uniquely determined by the vertex type of its central site. It would be more correct to take all possible higher-order vertex types [27], i.e. m-order vertex types related to neighbours located not further than m edge lengths from the site, but since their number grows quite rapidly with the order, the initial set of graphs would be too numerous and the generation of overlaps (see the next item) too time consuming.
2. Generate all possible overlaps of embeddings of the initial graphs in the tiling. It is difficult to estimate how the time of the generation depends on the number of initial graphs. Let us say a couple of words about this, however. We group graphs into generations so that the initial set of graphs constitutes the zeroth generation and the nth generation consists of overlaps of graphs from the $(n-1)$th and zeroth generations. Since the time for creating the nth generation depends on the product of numbers of graphs $g(0)$ from generation zero and $g(n-1)$ from generation $(n-1)$ starting from a too numerous zeroth generation should be avoided. The total number of overlaps grows rather slowly with $g(0)$, for large $g(0)$, and most of the computing time will be devoted to checking and rejecting graphs which occurred before. On the other hand, if we took too few initial patches, the covering of the lattice with them would be incomplete, there would be plenty of 'holes' not covered by any of the patches, and thus the series expansion would be marked by error. The rule of thumb is to take $g(0)$ not larger than 20 and choose the patches in such a way that their interiors differ as much as possible.

   Again, on the square lattice it is immediately clear that the overlaps are rectangles, because every rectangle can be constructed as an overlap of two other rectangles, whereas on the PT the shapes of graphs and their quantity depend on the initial set. To make things worse, we are not even sure that we obtain star graphs [24, pp 1–16], i.e., graphs without articulation points, because the initial graphs are not necessarily convex. Connected graphs consisting of multiple components will cause some difficulties due to the calculation of partition functions by the transfer-matrix method (see following items).
3. Generate all possible 'decorations' of graphs constructed in the previous step. Boundary conditions are important for calculating partition functions in the finite lattice method (FLM). Since expansion (3) is a low-temperature expansion, i.e. graphs g_r represent excitations from the ground state—they can be regarded as groups ('islands') of excited spins surrounded by a sea of unexcited, parallel spins—it is essential to know the graph decoration, i.e. vertex types of all sites including those at the boundary, when calculating partition functions. On regular lattices this problem is sorted out automatically; a finite portion from the lattice determines uniquely vertex types of all its sites, whereas finite portions from quasiperiodic lattices can have different decorations. This is in a way

similar to the issue of different 'boundary line fillings' discussed before; a finite patch of a quasiperiodic lattice does not determine uniquely vertex types of sites on its boundary.

Here we refrain from describing how the 'boundary line fillings' or 'decorations' of finite graphs are constructed. It would require a detailed discussion of construction methods of quasiperiodic lattices, in particular notions such as the 'cut-and-project' method or acceptance domains of graphs [32]. Let us only mention that there is an upper bound on the number of 'decorations' of an arbitrary graph. In other words, an arbitrary graph can be embedded in the quasiperiodic lattice in not more than several, usually five, different ways. Putting it in another way, we do not have to worry that the set of decorated graphs will grow to enormous quantities, which would make the procedure described here inapplicable in practice.

4. Calculate the contribution a_r of graph g_r in (3) in the following recursive way:

$$a_r = (g_r; G) - \sum_{r \subset p} a_p(g_r; g_p) \tag{4}$$

where the sum on the right-hand side runs over all graphs g_p in which g_r can be embedded.

5. Calculate logarithms of partition functions $\log Z(g_r)$ by the transfer-matrix method.

The transfer-matrix method. Here we have to distinguish two cases, namely the case when the graph has no articulation points (star graph) and the contrary (multicomponent graph). The latter is undoubtedly more complicated but fortunately it turns out that it takes place only in a minority of the graphs under consideration. Let us firstly discuss the case of a star graph. We can define a perimeter of the graph, i.e. a line consisting of edges each of which belongs only to one rhombi. The sum over spin configurations can be performed by moving a boundary line across the graph. At each stage the boundary line goes through a number, say k, of sites. For the Q-state Potts model we have Q^k different spin configurations on the boundary line. Now we define a Q^k-dimensional vector $Z(\sigma)$ consisting of partition functions calculated for the patch composed of sites from the boundary line, with a given spin configuration $\sigma = \{\sigma_1, \sigma_2, \ldots, \sigma_N\}$ assigned to them, and sites already traversed by the boundary line. Let us define $\tilde{x} = \exp(-\beta J)$ and $\tilde{y} = 1 - \exp(-\beta B/2)$. Then the initial values of $Z(\sigma)$ are given by

$$Z(\sigma) = \tilde{x}^a (1 - \tilde{y})^b \tag{5}$$

where

$$a = \sum_{p=1}^{N-1} \Delta(\sigma_p, \sigma_{p+1}) + \sum_{p=1}^{N} \mathcal{N}(p) \Delta(\sigma_p, 0) \qquad b = 2 \sum_{p=1}^{N} \Delta(\sigma_p, 0) \tag{6}$$

and $\mathcal{N}(p)$ denotes the valence of the boundary site p diminished by the number of edges from the undecorated graph which emanate from this site (see item 3 in section 3).

Shifting the boundary line corresponds to generating a new vector $Z'(\sigma')$ of partition functions from the old vector Z. There is a lot of ambiguity in shifting the boundary line by a given number of tiles. In our case it amounts, however, to considering only three kinds of movements, by one tile, by two tiles and a shift between two given boundary line configurations, which we discuss below. Placing the initial boundary line on the perimeter of the graph and moving it at each stage by a certain number of tiles, see figure 1, we have performed the sum over all configurations after reaching the final position of the boundary line (also lying on the perimeter).

Now we discuss the details of updating the partition functions for the two kinds of boundary line movements, see figure 2.

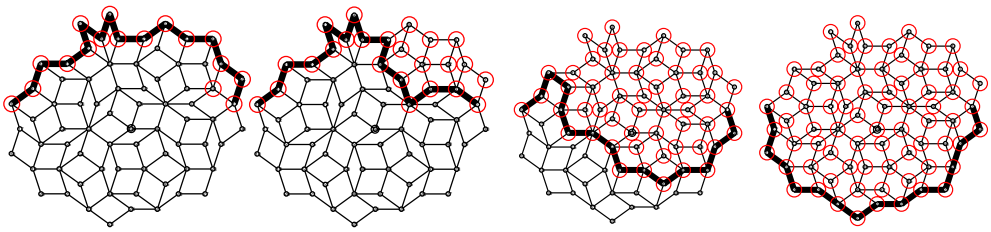

Figure 1. Shifting of a boundary line through a graph, from the initial (leftmost picture) to the final (rightmost picture), corresponding to calculating the partition function by the transfer-matrix method.

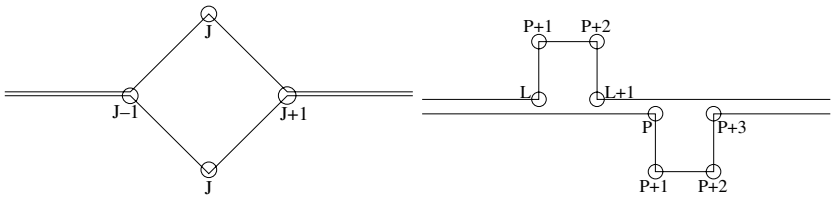

Figure 2. Two kinds of movements of the boundary line, by one tile (left) and by two tiles (right). In both cases, the lower part of the figure shows the old boundary line and the upper part the updated new boundary line. The labels of the circle-marked sites denote the number of the site both before (the lower part) and after updating (the upper part).

3.1. One-tile movement

For $1 \leqslant J \leqslant N$ we have

$$Z'(\sigma') = \tilde{x}^a (1-\tilde{y})^b \sum_{\sigma_J=1}^{q} Z(\sigma) \tag{7}$$

where $a = \Delta(\sigma'_{J-1}, \sigma'_J) + \Delta(\sigma'_J, \sigma'_{J+1})$ and $b = f\Delta(\sigma'_J, 0)$, $f = 2$.

3.2. Two-tile movement

For $1 \leqslant L < P \leqslant N$ we have

$$Z'(\sigma'_\rho) = \tilde{x}^a (1-\tilde{y})^b \sum_{\sigma_{P+1}=1}^{q} \sum_{\sigma_{P+2}=1}^{q} Z(\sigma) \tag{8}$$

where $a = \Delta(\sigma'_L, \sigma'_{P+1}) + \Delta(\sigma'_{P+1}, \sigma'_{P+2}) + \Delta(\sigma'_{P+2}, \sigma'_{L+1}) + \Delta(\sigma'_P, \sigma'_{P+3})$ and $b = f_1\Delta(\sigma'_{P+1}, 0) + f_2\Delta(\sigma'_{P+2}, 0)$ where $f_1 = f_2 = 2$, and the new spin configuration is permuted with respect to the old one $\sigma'_\rho = \{\sigma'_{\rho_1}, \sigma'_{\rho_2}, \ldots, \sigma'_{\rho_N}\}$ and

$$\rho_p = \begin{cases} p & p \leqslant L \\ P+1 & p = L+1 \\ P+2 & p = L+2 \\ p-2 & p \geqslant L+3 \end{cases}. \tag{9}$$

3.3. Shifting the boundary line to the final position

In most cases it is possible to displace the boundary line from the initial to the final position by a sequence of the movements defined above. Sometimes, however, we arrive at a dead end

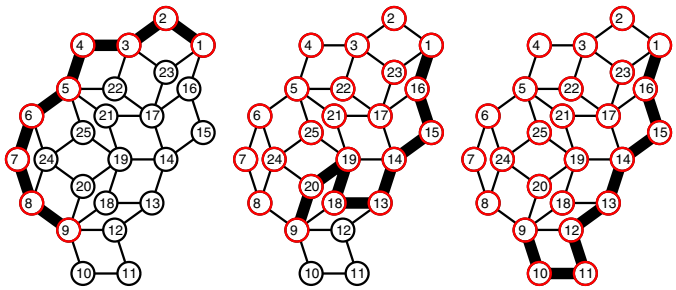

Figure 3. A boundary line (middle picture) which cannot be pushed forward by performing one of the movements discussed above. The initial and the final line configuration are shown at the left and at the right, respectively.

because none of the movements can be done, see figure 3. In this case, we have to shift the line directly to its final position by summing over all the spins which have not been taken into account yet. The formal prescription for updating $Z(\sigma)$ in this case reads

$$Z'\left(\sigma_{F_1},\ldots,\sigma_{F_9}\right)=\sum_{\sigma_{s_1},\sigma_{s_2},\sigma_{s_3}}\tilde{x}^a(1-\tilde{y})^b Z\left(\sigma_{B_1},\ldots,\sigma_{B_9}\right) \tag{10}$$

where $a=\sum_{j=1}^{6}\Delta\left(\sigma_{e_{j,1}},\sigma_{e_{j,2}}\right)$ and $b=2\sum_{j=1}^{3}\Delta\left(\sigma_{s_j},0\right)$ and $B=\{1,16,15,14,13,18,19,20,9\}$, $F=\{1,16,15,14,13,12,11,10,9\}$, $e=\{(9,10),(10,11),(11,12),(12,13),(12,9),(9,18)\}$ and $s=\{12,11,10\}$ denote the current and the final boundary lines, the edges and the sites, respectively, which were not taken into account yet.

In principle, it could be possible to consider an alternative movement where the boundary line changes length. In the case shown in figure 3 this corresponds, for example, to a contraction of the boundary line B which merges into a line B' shorter by two edges, where $F=\{1,16,15,14,13,18,9\}$. The updated partition-functions-vector has a different dimension, smaller by Q^2, and the updating recipe reads

$$Z'\left(\sigma_{B'_1},\ldots,\sigma_{B'_7}\right)=\tilde{x}^a(1-\tilde{y})^b\sum_{\sigma_{s_{20}},\sigma_{s_{19}}}Z\left(\sigma_{B_1},\ldots,\sigma_{B_9}\right) \tag{11}$$

where $a=\Delta(\sigma_9,\sigma_{18})$ and $b=\Delta(\sigma_{20},0)+\Delta(\sigma_{19},0)$. There is, however, one problem connected with such movements. At some stage, i.e. after a couple of update-steps, contractions of the boundary line have to be followed by its expansions. Moreover, there must be as many expansions as there were contractions because the boundary line in the end position has the same length as it had at the start. In the case shown in figure 3, such a sequence of boundary lines exists and it reads

$$\{1,16,15,14,13,18,19,20,9\}\Longrightarrow\{1,16,15,14,13,18,9\}$$
$$\Longrightarrow\{1,16,15,14,13,12,9\}\Longrightarrow\{1,16,15,14,13,12,11,10,9\}.$$

There is no certainty that in the generic case such a sequence of boundary lines exists, though. Therefore in our calculations we refrained from altering the dimension of the partition-functions-vector and worked only with boundary lines of fixed length. Moreover, the dead-end case occurs only in very few cases; from 264 relevant graphs in our computations it happened only in less than 9 cases all of which were graphs of relatively small size.

Can the transfer-matrix formalism (tmf) also be applied to the case of a multicomponent graph? The answer is affirmative because every connected graph can be dissected into its star

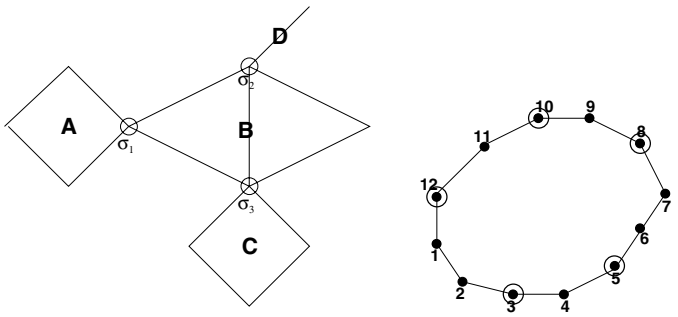

Figure 4. A multicomponent graph consisting of four star components (left) and the perimeter of a star graph with two isolated sites on the initial boundary line (consisting of sites from 1 to 7) and three isolated sites on the final boundary line (sites from 7 to 12) (right). The isolated sites are marked with circles.

graph components for which the tmf is applicable. Since, however, star graph components share certain sites at their boundaries, which we call in the following isolated sites, we have to calculate a whole set of partition functions with given spin values at isolated sites and combine them to get the partition function of the whole graph. In the following we assume the simplest case, namely, that every isolated site is shared by exactly two star components. This was indeed the case by our overlap graphs. Let us explain the procedure for the case of a graph depicted in figure 4. The partition function Z can be built up from partition functions $Z_A(\sigma_1)$, $Z_B(\sigma_1, \sigma_2, \sigma_3)$, $Z_C(\sigma_3)$ and $Z_D(\sigma_2)$ corresponding to star components A, B, C and D with isolated spins σ_1, σ_2 and σ_3

$$Z = \sum_{\sigma_1,\sigma_2,\sigma_3} Z_A(\sigma_1) Z_B(\sigma_1, \sigma_2, \sigma_3) Z_C(\sigma_3) Z_D(\sigma_2). \tag{12}$$

Now, the problem consists in calculating partition functions for a star graph with specified spins at isolated sites located at the boundary. Assume that we have p isolated sites j_k, $k = 1, \ldots, p$, located at the initial boundary line and q isolated sites l_k, $k = 1, \ldots, q$, at the final boundary line, respectively, see figure 4. The calculation of $Z\left(s_{j_1}, \ldots, s_{j_p}, s_{l_1}, \ldots, s_{l_q}\right)$ amounts to repeating the tmf Q^{p+q} times and modifying the initial and the final partition function set by setting certain entries to zero. We replace the initial partition function set by

$$\left[\prod_{k=1}^{p} \delta\left(\sigma_{j_k}, s_{j_k}\right)\right] Z(\sigma_1, \ldots, \sigma_N) \qquad \text{for given} \quad s_{j_1}, \ldots, s_{j_p} \tag{13}$$

and the final partition function set is multiplied by $\prod_{k=1}^{q} \delta\left(\sigma_{l_k}, s_{l_k}\right)$ again for a given spin configuration $s_{l_1}, \ldots, s_{l_q}$. Another slight modification which is required consists in setting the factors f, f_1 and f_2 entering in the exponent b in equations (7) and (8) according to whether the site is isolated (one) or not (two).

4. Series expansion of the free energy, magnetization and field derivatives of the magnetization

We have performed calculations for a set of graphs constructed in the following way. We cut off seven fairly round-shaped patches from the PT so that the central sites of the patches had different vertex types and their perimeter lengths were not larger than 40 edge lengths. Then

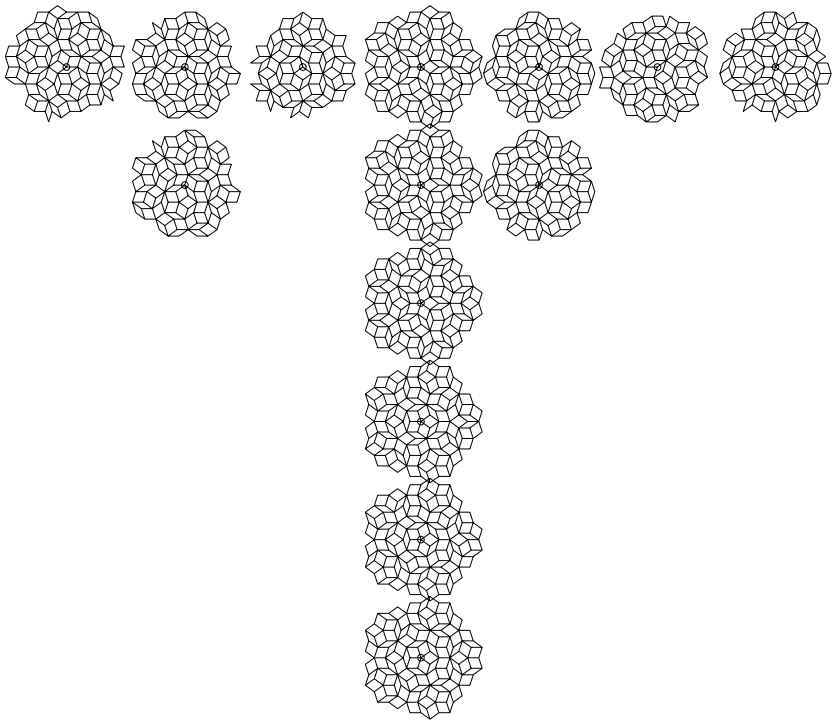

Figure 5. Patches from the Penrose lattice used as input for the FLM calculations. The columns contain all possible 'boundary line fillings' of seven patches the central sites of which correspond to seven different vertex types.

we enlarged the set of patches by all possible 'boundary line fillings' obtaining in effect 14 patches, see figure 5. In the next step, we constructed all possible graphs contributing to the expansion in the recursive way described in section 3. Their number turned out to be 8688. This part of computations was rather tedious, up to 2 weeks on a SunOS machine, because in generating graph overlaps many graphs turned up repeatedly and had to be rejected. In the next step we generated 'decorations' of graphs, i.e. we determined vertex types of all sites of the graph including those on its boundary (see item 3 in section 3). Since the graphs could have several decorations, the number of graphs we have to deal with increased to 36 480. Now we were ready to compute the coefficients a_r entering in (3) which appeared to be different from zero only for a small fraction of all graphs, namely for 264 graphs. This is not a surprising result since on the square lattice the vast majority of rectangles used in the expansion yields zero coefficients as well [26]. Fortunately, most of the relevant graphs here were star graphs (only 30 graphs did not have this property) so we could easily compute the free energies $\log Z(g_r)$ entering in (3) in the way described in section 3. There were, however, some awkward multicomponent graphs for which partition function computations were more tedious. The series expansion is shown beneath.

After reordering the expansion (3), i.e. collecting together terms with the same power of $\tilde{y}$, the free energy $F(\tilde{x}, \tilde{y})$ takes the form

$$F(\tilde{x}, \tilde{y}) = \log Z(\mathcal{G}) = F_0(\tilde{x}) + F_1(\tilde{x})\tilde{y} + F_2(\tilde{x})\tilde{y}^2 + \cdots = \sum_{n=0}^{\infty} F_n(\tilde{x})\tilde{y}^n. \quad (14)$$

Quantities such as the spontaneous magnetization $M(\tilde{x})$, susceptibility $\chi(\tilde{x})$ and field derivatives of the susceptibility $\chi^{(n)}(\tilde{x}) = \mathrm{d}^n\chi(\tilde{x})/\mathrm{d}\tilde{y}^n$ can be expressed as linear combinations of the polynomials $F_n(\tilde{x})$

$$\begin{aligned}
&M(\tilde{x}) = \mathrm{d}F(\tilde{x},\tilde{y})/\mathrm{d}B|_{B=0} = F_1(\tilde{x})\\
&\chi(\tilde{x}) = \mathrm{d}^2F(\tilde{x},\tilde{y})/\mathrm{d}B^2|_{B=0} = 2F_2(\tilde{x}) - F_1(\tilde{x})\\
&\chi^{(1)}(\tilde{x}) = \mathrm{d}^3F(\tilde{x},\tilde{y})/\mathrm{d}B^3|_{B=0} = 6F_3(\tilde{x}) - 6F_2(\tilde{x}) + F_1(\tilde{x})\\
&\chi^{(2)}(\tilde{x}) = \mathrm{d}^4F(\tilde{x},\tilde{y})/\mathrm{d}B^4|_{B=0} = 24F_4(\tilde{x}) - 36F_3(\tilde{x}) + 14F_2(\tilde{x}) - F_1(\tilde{x}).
\end{aligned} \tag{15}$$

5. Verification of correctness of the computed expansion

There is a duality relation connecting the low-temperature expansion of the Ising model on the lattice $\mathcal{G}$ to the high-temperature expansion on the dual lattice $\mathcal{D}$, which takes the following form:

$$Z_{\mathcal{G}}(x,y) = \exp\beta(MJ+NB)\tilde{Z}_{\mathcal{G}}(x,y) = 2^N(\cosh\beta J)^M(\cosh\beta B)^N\tilde{Z}_{\mathcal{D}}(w,h) \tag{16}$$

where the low-temperature variables are $x = \exp\{-2\beta J\}$, $y = \exp\{-\beta B\}$ and the high-temperature ones are $w = \tanh\{\beta J\}$, $h = \tanh\{\beta B\}$. In the field-free case $h = 0$, the high-temperature expansion of $\tilde{Z}_{\mathcal{D}}(w,0)$ can be expressed as the square root of the determinant of a $2M \times 2M$ complex matrix [15, 28], which for periodic lattices amounts to calculating a finite-dimensional determinant, the dimension of which is of the order of the size of the unit cell. Therefore, the free energy expansion in variable x can be calculated by taking logarithms of equation (16):

$$F = \lim_{N\longrightarrow\infty}\frac{1}{N}\log Z_{\mathcal{G}}(x) = \log 2 - \frac{q}{4}\log(1-w^2) + \log\tilde{Z}_{\mathcal{D}}(w) \tag{17}$$

where $q = \lim_{N\longrightarrow\infty} 2M/N$ is the mean coordination number. The expansion of the last term on the right-hand side

$$\log\tilde{Z}_{\mathcal{D}}(w) = \sum_{n=3}^{\infty} g_n w^n \tag{18}$$

is obtained from Kac–Ward determinants for large enough PAs of the Penrose lattice, see [15] for a detailed explanation. In table 2, we show the expansion coefficients g_n for successive PAs together with the coefficients of $F_0(x)$ (see (14)) obtained by the FLM. The data for the highest approximants are quite close to those for the FLM; the relative discrepancies for $n = 3, \ldots, 21$ are equal to -12.2%, -0.2%, 5.3%, -10.2%, -15.6%, -21.0%, -6.2%, 47.7%, -0.4%, -7.8%, -6.6%, 8.8%, 18.8%, 0.6%, -10.5%, -15.0%, -16.1%, -11.9%, -10.1% and in most cases do not exceed 10%. In addition, both data sets depend on n in a similar way. Indeed, assuming known values for the critical point $x_c = 0.434\,269$ and the critical exponent $\alpha = 2$, we define the sequence r_n in the following way:

$$r_n = g_n/g_{n-1} - 1/x_c(1-(\alpha+1)/n). \tag{19}$$

This sequence approaches zero, $r_n \longrightarrow 0$, for large n, see [24, pp 87–199]. If we now compare the sequences from both the PA coefficients and the FLM coefficients, we see that the relative discrepancies except for $n = 5, 10, 12$ are all smaller than 10% as well.

The lowest coefficients of our expansions can also be calculated exactly by counting graphs on the dual Penrose lattice. Here we confine ourselves to the free energy and the

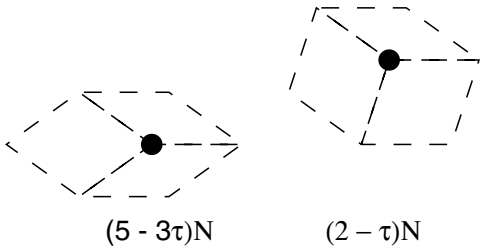

Figure 6. Graphs from Penrose lattice contributing to the coefficient $h_{3,1}$ and their embedding numbers expressed through $\tau = (\sqrt{2} - 1)/2$. The dual graphs are constructed by connecting midpoints of rhombi abutting at bonds terminated by filled circles.

Table 1. Expansion coefficients of the magnetization $M(x)$, susceptibility $\chi(x)$ and its field derivatives $\chi^{(1)}(x)$, $\chi^{(2}(x)$ obtained from the FLM.

	$M(x)$	$\chi(x)$	$\chi^{(1)}(x)$	$\chi^{(2)}(x)$
g_3	−1.182	2.364	−4.728	−38.414
g_4	−0.180	0.361	0.721	−5.861
g_5	−1.255	3.989	−9.457	−67.231
g_6	−3.706	15.680	−39.622	−268.284
g_7	−10.711	64.593	−172.355	−1121.644
g_8	−14.694	123.316	−340.560	−2162.536
g_9	−13.853	171.487	−486.757	−3032.051
g_{10}	−17.478	284.234	−817.746	−5046.599
g_{11}	−77.4685	1090.3969	−3116.2537	−19322.1507
g_{12}	−250.04	3723.64	−10670.9	−66041.4
g_{13}	−514.05	8998.96	−25968.8	−159951.9
g_{14}	−797.74	17776.65	−51734.5	−316815.7
g_{15}	−1473.51	39523.94	−115624.8	−705571.7
g_{16}	−3899.04	107019.97	−313261.8	−1910877.8
g_{17}	−9661.10	278241.01	−815400.8	−4969991.0
g_{18}	−18945.45	633794.24	−1863491.8	−1133297.3
g_{19}	−33814.06	1387869.95	−4.095981.7	−2484688.6
g_{20}	−70998.11	3263830.44	−9649495.1	−5846579.9
g_{21}	−172967.34	8082525.39	−23901641.5	−144796341.7
g_{22}	−401040.95	1957029.14	−57908792.2	−350667957.7
g_{23}	−848957.34	45837936.7	−135815895.5	−821699397.1
g_{24}	−1794310.13	107642260.6	−319338161.6	−1930404487
g_{25}	−4051809.18	258546263.5	−767535172.1	−4637671710

magnetization expansions. We compute their first four non-zero coefficients and show that they are indeed close to those from tables 1 and 2. We start from the low-temperature expansion

$$x^{M/2} y^N Z_{\mathcal{G}}(x, y) = \tilde{Z}_{\mathcal{G}}(x, y) = \sum_{n,m} h_{n,m} x^n y^{2m} \tag{20}$$

with $h_{n,m}$ counting graphs, in general multicomponent graphs, from dual lattice consisting of m sites and n bonds on the perimeter. It is readily seen from figures 6–9 that for the Penrose

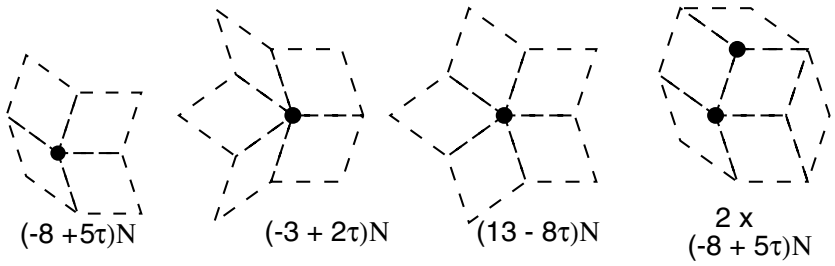

Figure 7. The same as above, corresponding to coefficients $h_{4,1}$ (three on the left) and $h_{5,1}$ (last on the right).

Table 2. Expansion coefficients for free energy (18) for PAs $m = 3, \ldots, 9$ of the dual Penrose lattice with M edges in the unit cell. In the right-most column are coefficients obtained by the finite lattice expansion. The entries marked by '–' denote the case where, due to large computational effort, no data were available. The numbers g_n approach the expansion coefficients for the dual Penrose lattice when $m \longrightarrow \infty$.

m	3	4	5	6	7	8	9	
$2M$	304	796	2084	5456	14284	37396	97904	
g_3	0.5132	0.5176	0.5259	0.5279	0.5279	0.5277	0.5266	0.5910
g_4	0.1053	0.1106	0.0940	0.0902	0.0902	0.0906	0.0900	0.0902
g_5	0.4868	0.4824	0.4722	0.4707	0.4716	0.4672	0.4712	0.4460
g_6	0.8355	0.8116	0.8234	0.8262	0.8262	0.8273	0.8207	0.9047
g_7	1.5658	1.5477	1.5873	1.5894	1.5858	1.5467	1.5746	1.8206
g_8	1.3289	1.3518	1.3580	1.3596	1.3587	1.3144	1.3443	1.6272
g_9	0.7368	0.7605	0.6379	0.6452	0.6551	0.6159	0.6483	0.6883
g_{10}	1.0987	0.7286	0.6180	0.6078	0.6054	0.5948	0.5732	0.2998
g_{11}	5.5921	4.8492	5.0768	5.0249	4.9812	4.7844	4.8631	4.8807
g_{12}	14.3213	14.7944	15.2147	15.2147	15.1629	14.4285	14.8233	15.9759
g_{13}	24.0789	26.4623	26.4607	26.5257	26.6334	25.1886	–	26.8614
g_{14}	33.3618	32.9548	32.0010	31.9245	32.0060	29.5740	–	26.979
g_{15}	58.9491	50.7568	48.7386	48.0850	47.7786	42.8330	–	34.7744
g_{16}	134.8618	129.4246	128.2087	127.5097	127.0104	115.1099	–	114.4562
g_{17}	270.2105	287.3266	291.4299	292.4663	292.7278	269.0166	–	297.2675
g_{18}	413.0614	427.7404	432.9875	435.5210	436.5489	398.7356	–	458.5212
g_{19}	573.6842	495.4975	474.8081	474.0257	473.8073	415.9446	–	482.8437
g_{20}	1105.3993	928.3412	872.2088	866.5213	864.7229	753.3294	–	843.1892

lattice the non-zero coefficients take following values:

$$\begin{aligned}
&h_{3,1} = (7-4\tau)N \qquad && h_{4,1} = (-8+5\tau)N \\
&h_{5,1} = (10-6\tau)N \qquad && h_{5,2} = (-16+10\tau)N \\
&h_{6,1} = (-21+13\tau)N \qquad && h_{6,3} = (-8+5\tau)N \\
&h_{6,2} = (22-13\tau)N + (7-4\tau)N((7-4\tau)N-1) \\
&h_{7,1} = (13-8\tau)N \qquad && h_{7,4} = (-8+5\tau)N \\
&h_{7,3} = (79-48\tau)N \qquad && h_{7,2} = (-63+39\tau)N + (7-4\tau)(-8+5\tau)N^2.
\end{aligned} \tag{21}$$

Let us note that disjoint, two-component graphs (figures 9–10) also contribute to coefficients $h_{6,2}$ and $h_{7,2}$, thus the coefficients are second degree polynomials in N.

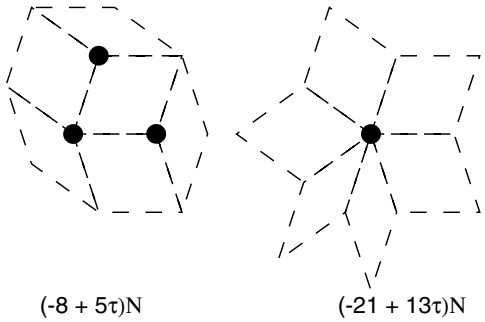

Figure 8. Graphs contributing to the coefficients $h_{6,3}$ (left) and $h_{6,1}$ (right).

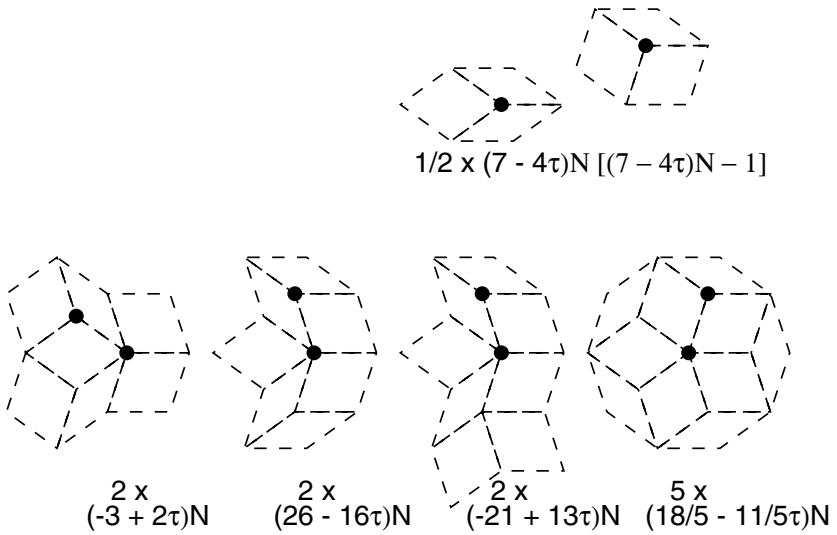

Figure 9. Graphs contributing to the coefficient $h_{6,2}$.

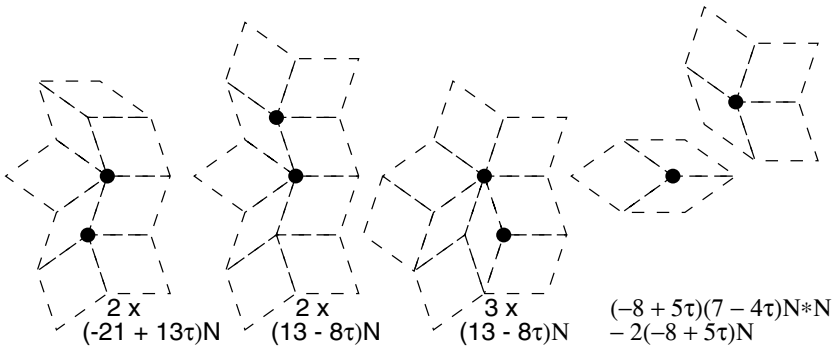

Figure 10. Graphs contributing to the coefficient $h_{7,2}$.

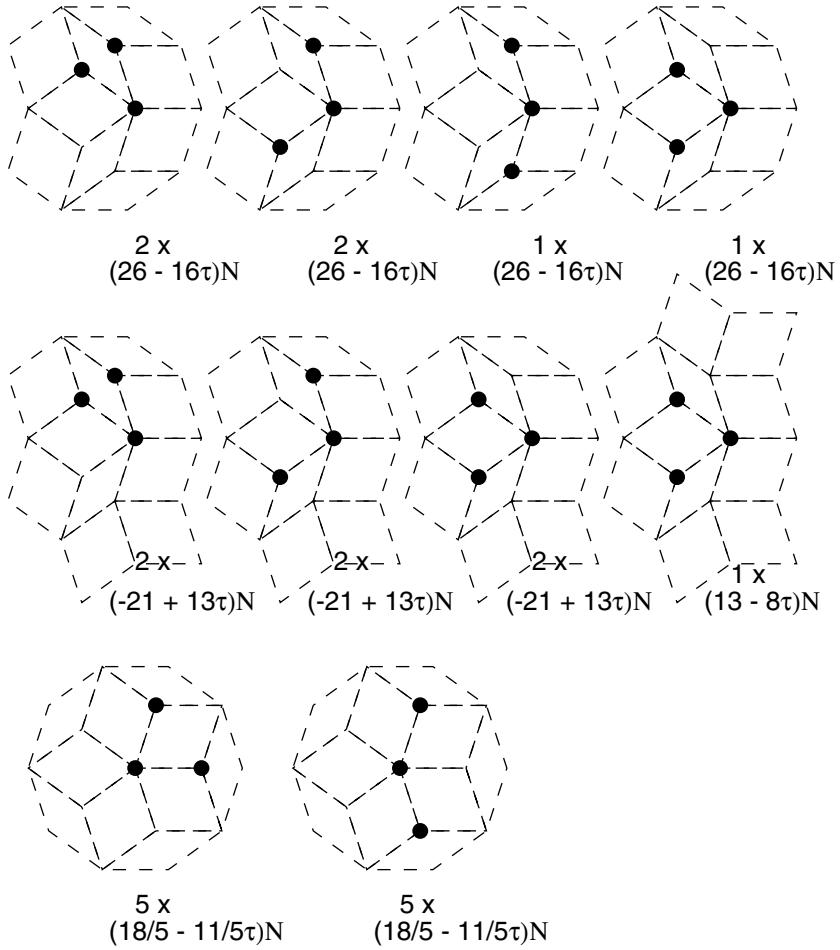

Figure 11. Graphs contributing to the coefficient $h_{7,3}$.

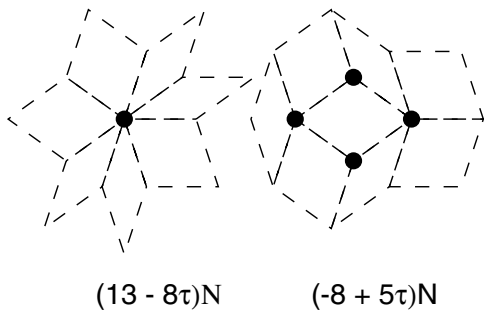

Figure 12. Graphs contributing to the coefficients $h_{7,1}$ (left) and $h_{7,4}$ (right).

If we now insert the coefficients from (21) into the definitions of the magnetization $M(x)$ and the susceptibility $\chi(x)$

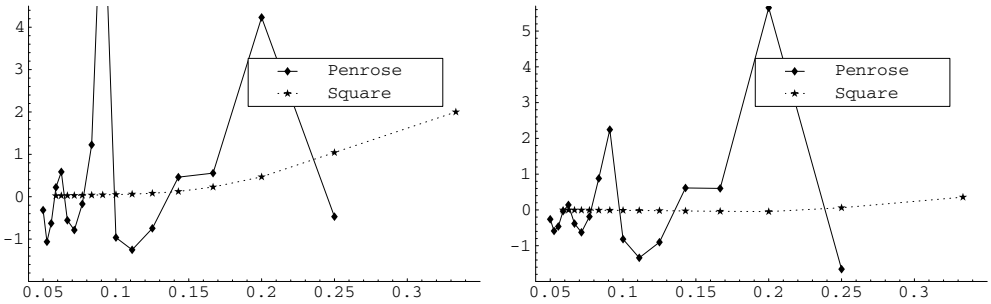

Figure 13. Plots of residues r_n (19) as a function of $1/n$ for the free energy (left) and the magnetization (right) on the Penrose and the square lattice, respectively. In both cases we took the critical exponents $\alpha = 2$ and $\beta = 1/8$.

$$M(x) = \frac{1}{N}\frac{\mathrm{d}\log[Z_{\mathcal{G}}(x,y)]}{\mathrm{d}B}\bigg|_{B=0} = 1 - \frac{1}{N}y\frac{\mathrm{d}\log[\tilde{Z}_{\mathcal{G}}(x,y)]}{\mathrm{d}y}\bigg|_{y=1}$$
$$\chi(x) = \frac{1}{N}\frac{\mathrm{d}M(x)}{\mathrm{d}B}\bigg|_{B=0} = \frac{1}{N}y\frac{\mathrm{d}}{\mathrm{d}y}y\frac{\mathrm{d}\log[\tilde{Z}_{\mathcal{G}}(x,y)]}{\mathrm{d}y}\bigg|_{y=1} \tag{22}$$

we obtain following expansions:

$$F(x) = 0.5279x^3 + 0.0902x^4 + 0.4721x^5 + 0.8262x^6 + 1.583\,59x^7 + O(x^8)$$
$$M(x) = 1 - 1.0557x^3 - 0.1803x^4 - 1.3049x^5 - 3.4164x^6 - 9.252\,33x^7 + O(x^8)$$
$$\chi(x) = 2.1115x^3 + 0.3607x^4 + 4.0526x^5 + 14.6099x^6 + 55.6843x^7 + O(x^8)$$
$$\chi^{(1)}(x) = 4.2229x^3 + 0.7214x^4 + 13.8761x^5 + 64.6563x^6 + 341.449x^7 + O(x^8)$$

which conform quite well to the values from table 1. Indeed, the relative differences between both sets of coefficients do not exceed 10% in any case.

6. Asymptotic analysis of the series expansions

Now the problem consists in extracting critical exponents from the obtained expansions. The simplest approach, the ratio method, in which one examines the asymptotically linear dependence of ratios g_n/g_{n-1} (19) on $1/n$ and obtains x_c and α from linear regression, is inapplicable in this case because of the slow convergence of series. Indeed, the residues r_n (19) are much larger than those for the square lattice and alternate in sign, see figures 13 and 14, that makes the asymptotic analysis difficult. This approach requires knowledge of x_c which is known from other works [8, 29] only with a limited accuracy. Applying the Padé method gives much more satisfactory results. Assuming that our thermodynamic functions $F(x)$ behave in the vicinity of the critical point x_c as $F(x) \simeq (1 - x/x_c)^{-\alpha}A(x)$, it is readily seen that functions $G_0(x)$ and $G_1(x)$ behave asymptotically as follows:

$$G_0(x) = \frac{\mathrm{d}}{\mathrm{d}x}\left(\log\frac{\mathrm{d}F(x)}{\mathrm{d}x}\right)\Big/\frac{\mathrm{d}}{\mathrm{d}x}(\log F(x)) \simeq \frac{\alpha+1}{\alpha} + O(x - x_c) \tag{23}$$

$$G_1(x) = (x - x_c)\frac{\mathrm{d}}{\mathrm{d}x}(\log F(x)) \simeq \alpha + O(x - x_c). \tag{24}$$

Constructing Padé approximants to $G_0(x)$ and $G_1(x)$ and evaluating them at $x = x_c = 0.434\,269$ usually yields a reasonable estimation of α, even if x_c is only known with a

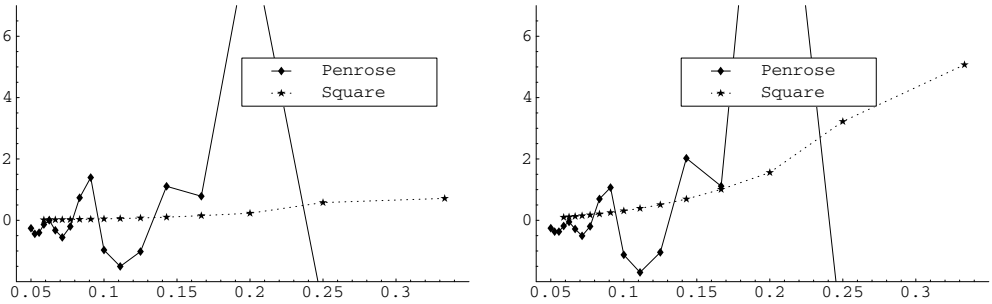

Figure 14. As before for the susceptibility (left) and the field derivative of susceptibility (right). In both cases we took the critical exponents $\gamma = -7/4$ and $\delta = -29/8$.

Table 3. Estimates of the magnetization critical exponent β by means of Padé approximants $[n, m]$ to functions $G_0(x)$ and $G_1(x)$ (24) constructed from the expansion to an order of 20 for the square and Penrose lattice, respectively. Entries marked by asterisks differ strongly from square-lattice exponents.

	Approximant											
	$[n, n-1]$				$[n, n]$				$[n, n+1]$			
	Penrose		Square		Penrose		Square		Penrose		Square	
n	$G_0(x)$	$G_1(x)$	$G_0(x)$	$G_1(x)$	$G_0(x)$	$G_1(x)$	$G_0(x)$	$G_1(x)$	$G_0(x)$	$G_1(x)$	$G_0(x)$	$G_1(x)$
8	0.146	0.133	0.125	0.125	0.138	0.131	0.125	0.125	0.138	0.137	0.125	0.125
9	0.137	0.172*	0.125	0.125	0.138	0.129	0.125	0.125	0.138	0.130	0.125	0.125
10	0.138	0.130	0.125	0.125	0.138	0.129	0.125	0.125	0.138	0.130	0.125	0.125
11	0.136	0.130	0.125	0.125	0.138	0.129	0.125	0.125	0.138	0.139	0.125	0.125
12	0.138	0.663*	0.125	0.125	0.138	0.131	0.125	0.125	0.138	0.133	0.125	0.125
13	0.137	0.133	0.125	0.125	0.138	0.133	0.125	0.125	0.134	0.133	0.125	0.125
14	0.170*	0.132	0.125	0.125	0.134	0.133	0.125	0.125	0.134	0.133	0.125	0.125
15	0.125	0.133	0.125	0.125	0.150	0.131	0.125	0.125	0.146	0.531*	0.125	0.125

Table 4. As before for the susceptibility critical exponent γ.

	Approximant											
	$[n, n-1]$				$[n, n]$				$[n, n+1]$			
	Penrose		Square		Penrose		Square		Penrose		Square	
n	$G_0(x)$	$G_1(x)$	$G_0(x)$	$G_1(x)$	$G_0(x)$	$G_1(x)$	$G_0(x)$	$G_1(x)$	$G_0(x)$	$G_1(x)$	$G_0(x)$	$G_1(x)$
15	−0.659*	−1.678	−1.742	−1.748	3.047*	−1.56	−1.742	−0.001*	−1.273	−1.363	−1.743	−1.749
16	−2.128	0.321*	−1.744	−1.749	−3.458*	−1.36	−1.742	−1.749	−2.537*	−1.363	−1.742	−1.749
17	−2.733*	−1.259	−1.742	−1.749	−4.931*	−3.859*	−1.742	−0.001*	−1.642	−1.244	−1.757	−1.748
18	−2.002	−1.131*	−1.737	−1.748	−1.875	−1.035*	−1.736	−1.748	−1.328	−1.527	−1.736	−1.748
19	−1.972	−1.164*	−1.736	−1.747	−0.482*	−1.455	−1.736	0.*	−0.865*	−1.509	−1.732	−1.747
20	−0.958*	−2.219	−1.738	−1.747	−0.592*	−0.589*	−1.716	−1.747	−1.129*	−0.387*	−1.716	−1.747
21	−1.664	−0.404*	−1.716	−1.747	3.342*	−0.558*	−1.716	0.*	−2.749*	−0.712*	−1.699	−1.588

moderate accuracy. Results of this analysis, shown in tables 3 and 4, are fairly close to the square lattice exponents. The sequence of Pade approximants is quite stable, except for few cases marked by asterisks. Whenever the square lattice results converged, Penrose data did as well.

Table 5. Biased estimates of the critical point $x_c = \exp(-2\beta_c)$ obtained from the magnetization expansion to an order of 20 for the square and Penrose lattice, respectively.

	Approximant $[n, n-1]$		Approximant $[n, n]$		Approximant $[n, n+1]$	
n	Penrose	Square	Penrose	Square	Penrose	Square
8	0.432	0.414	0.433	0.414	0.432	0.414
9	0.432	0.414	0.432	0.414	0.432	0.414
10	0.432	0.414	0.432	0.414	0.432	0.414
11	0.443	0.414	0.435	0.414	0.434	0.414
12	0.433	0.414	0.433	0.414	0.433	0.414
13	0.434	0.414	0.433	0.414	0.434	0.414
14	0.431	0.414	0.435	0.414	0.432	0.414

On the other hand, we can compute biased estimates of x_c, assuming known values of critical exponents. Indeed, the appropriate poles of Padé approximants to the function $(F(x))^{1/\alpha}$ should give rapidly convergent sequence of estimates of x_c. These sequences for the magnetization expansion are shown in table 5. In most cases, the data do not deviate more than 1% from the exact values $x_c = 0.434\,269$ (Penrose lattice [29]) and $x_c = \sqrt{(2)} - 1$ (square lattice).

We can therefore claim that the data support the claim that the quasiperiodic Ising model under consideration belongs to the square lattice (Onsager) universality class.

7. Concluding remarks and outlook

The aim of this work was to analyse a quasiperiodic Ising model by means of graphical series expansions. Although the work is only devoted to the Penrose lattice, the same formalism can be easily applied to other 2D quasiperiodic lattices obtained by the 'cut-and-project' method from higher dimensions, i.e. lattices with octagonal or dodecagonal symmetry [31]. We calculated low-temperature expansions of the free energy, magnetization and the susceptibility to an order of 25 and extracted the respective critical exponents. We note that we did not obtain exact values for the coefficients and the exponents. Both of them are marked by errors, which however do not exceed 15% in most cases. This feature is rather unusual for series expansions on regular lattices where the coefficients are exact to a given order which is determined by the size of patches used for calculations. This deserves further comment. Following are the two sources of errors in our method:

(1) There are always graphs which cannot be embedded in any of the patches used in the calculations.
(2) The FLM consists in covering and probing the lattice with a finite set of patches. Since the lattice is irregular, in particular, not periodic, there can always be 'holes', i.e. groups of sites, associated with graphs on the dual lattice, which are not covered by any of the patches. Such incomplete covering with only a single patch is shown in figure 15. Consequently, even if the patches are large there can always be few small graphs which cannot be embedded into them and which produce an error in even the lowest order coefficients.

Even though the above explanation seems to be convincing, the fact that already the lowest coefficients g_3 (see table 2) are marked by a considerable error, $\simeq 12\%$, is slightly worrying. How can we examine quantitatively the source of this error? The coefficient g_3 would be

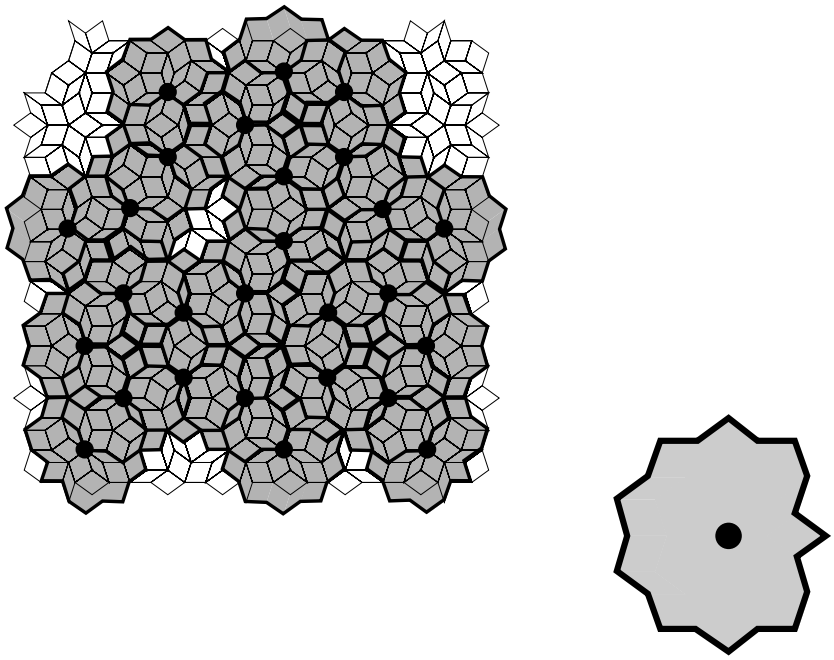

Figure 15. Covering of a fragment of the Penrose lattice (left) with copies of a patch consisting of 18 thick and 10 thin rhombi (right). Central sites of patches are marked by black dots. One can see that the covering is not complete, there are holes not covered by any of the patches.

correct if every site of valence 3 (with three neighbours) was embedded in at least one of the 14 round-shaped start patches shown in figure 5. This condition can be examined in terms of the 'cut-and-project' method, in particular through the acceptance domains (ADs) of the patches. The AD of a patch G denoted by $\mathcal{A}(G)$ is, in the case of the Penrose lattice, a planar convex geometrical figure the area of which is proportional to the embedding number of the patch G in the lattice. For example, the embedding numbers of graphs in (figures 6–12) were obtained by analysing the corresponding acceptance domains. A site of valence three g can be embedded in a graph $G = \{\vec{r}_i | i = 1, \ldots, p\}$ if and only if the acceptance domain $\mathcal{A}(G)$ after an appropriate shift by $\vec{s}_\perp$ belongs to $\mathcal{A}(g)$. The shift cannot be random; it has to be chosen in such a way that its parallel component $\vec{s}_\parallel$ corresponds to one of the vectors from G. In other words, the following condition:

$$\exists_{i=1,\ldots,14}\left[\mathcal{A}(G^{(i)}) - \vec{s}_\perp^{(i)}\right] \subset \mathcal{A}(g) \tag{25}$$

where $\vec{s}_\parallel^{(i)} \subset G^{(i)}$ is equivalent to the coefficient g_3 having the correct value. Here we refrain from checking this condition but it is not difficult to do it and nor would it be if the set of start patches was changed. Besides, since the size of $\mathcal{A}(G)$ decreases rapidly when the number of sites of G increases, it is not obvious that for every set of fairly large start patches $G^{(i)}$ the condition will be satisfied. Indeed, even a glimpse of figure 15 tells us that the condition may not be satisfied; a site of valence 3 belongs to the white-coloured part of the lattice, i.e., is not covered by any copy of the patch.

The next step in our research is to analyse the quasiperiodic Q-state Potts models, especially for $Q = 3, 4$ because the Harris-Luck criterion implies that quasiperiodic order should be strong enough to alter the critical behaviour in these cases. The main problem here consists in calculating partition functions for finite patches. This can be done, for instance,

by improving the FLM [30] where the expansion for a particular Q is obtained from partition functions with smaller Q values. Work in this direction is in progress.

Acknowledgments

PR thanks Des Johnston for discussions and an attentive proof reading of the paper. This work has been supported by a European Community IHP network HPRN-CT-1999-00161 'EUROGRID'.

References

[1] Schechtman D, Blech I, Gratias D and Cahn J W 1984 Metallic phase with long-range orientational order and no translational symmetry *Phys. Rev. Lett.* **53** 1951–3

[2] Grimm U and Baake M 1997 *The Mathematics of Long-Range Aperiodic Order (NATO ASI Series C 489)* ed R V Moody (Dordrecht: Kluwer) pp 199–237

[3] Luck J M 1993 A classification of critical phenomena on quasicrystals and other aperiodic structures *Europhys. Lett.* **24** 359–64

[4] Repetowicz P and Wolny J 1998 Diffraction pattern calculations for a certain class of N-fold quasilattices *J. Phys. A: Math. Gen.* **31** 6873–86

[5] Nischke K-P and Danzer L 1996 A construction of inflation rules based on n-fold symmetry *Discrete Comput. Geom.* **15** 221–36 (*Preprint* Zentralblatt MATH 849.52016)

[6] Hermisson J, Grimm U and Baake M 1997 Aperiodic Ising quantum chains *J. Phys. A: Math. Gen.* **30** 7315–35

[7] Okabe Y and Niizeki K 1988 Monte Carlo simulation of the Ising model on the Penrose lattice *J. Phys. Soc. Japan* **57** 16–9

[8] Sørensen E S, Jarić M V and Ronchetti M 1991 Ising model on the Penrose lattice: boundary conditions *Phys. Rev.* B **44** 9271–82

[9] Ledue D, Landau D P and Teillet J 1995 Static critical behaviour of the ferromagnetic Ising model on the quasiperiodic octagonal tiling *Phys. Rev.* B **51** 12523–30

[10] Redner O and Baake M 2000 Invaded cluster algorithm for critical properties of periodic and aperiodic planar Ising models *J. Phys. A: Math. Gen.* **33** 3097–109

[11] Penrose R 1974 The role of aesthetics in pure and applied mathematical research *Bull. Inst. Math. Appl.* **10** 266–71

de Bruijn N G 1981 Algebraic theory of Penrose's non-periodic tilings of the plane: I. Indagationes Mathematicae *Proc. K. Ned. Akad. Wet.* A **84** 39–52

de Bruijn N G 1981 Algebraic theory of Penrose's non-periodic tilings of the plane: II. Indagationes Mathematicae *Proc. K. Ned. Akad. Wet. Ser.* A **84** 53–66

[12] Bose I 1987 Renormalization group (RG) study of the Ising model on higher-dimensional ($d > 1$) quasi-lattices *Phys. Lett.* A **123** 224–6

[13] Aoyama H and Odagaki T 1987 Eight-parameter renormalization group for Penrose lattices *J. Stat. Phys.* **48** 503–11

Aoyama H and Odagaki T 1988 Renormalization group analysis of the Ising model on two-dimensional quasi-lattices *Int. J. Mod. Phys.* B **2** 13–35

[14] Abe R and Dotera T 1989 High temperature expansion for the Ising model on the Penrose lattice *J. Phys. Soc. Japan* **58** 3219–26

Dotera T and Abe R 1990 High temperature expansion for the Ising model on the dual Penrose lattice *J. Phys. Soc. Japan* **59** 2064–77

[15] Repetowicz P, Grimm U and Schreiber M 1999 High-temperature expansion of quasiperiodic Ising models *J. Phys. A: Math. Gen.* **32** 4397–418

[16] Domb C 1989 *Phase Transitions and Critical Phenomena* vol 13, ed C Domb and J L Lebowitz (London: Academic)

[17] Repetowicz P 2000 Theoretical investigations of magnetic and electronic properties of quasicrystals *PhD Thesis* Technische Universität Chemnitz, Germany webpage html://www.tu-chemnitz.de/physik/ARCHIV/PROMOT

[18] Wu F Y 1982 The Potts model *Rev. Mod. Phys.* **54** 235–67

[19] Chen S, Ferrenberg A M and Landau D P 1995 Monte Carlo simulation of phase transitions in a two-dimensional random-bond Potts model *Phys. Rev.* E **52** 1377–86

[20] Chatelain C, Berche P E and Berche B 1998 Second-order phase transition induced by deterministic fluctuations in aperiodic eight-state Potts model *Phys. Rev. Lett.* **80** 297
[21] Olson T and Young A P 1999 Monte Carlo study of the critical behavior of random bond Potts models *Phys. Rev.* B **60** 3428–34
[22] Roder A, Adler J and Janke W 1998 High-temperature series analysis of 2D random-bond Ising ferromagnets *Phys. Rev. Lett.* **80** 4697–700
[23] Janke W and Johnston D 2000 Ising and Potts models on quenched random gravity graphs *Nucl. Phys.* B **578** 681–98
[24] Domb C 1974 *Phase Transitions and Critical Phenomena* vol 3, ed C Domb and J L Lebowitz (London: Academic)
[25] Hijmans J and De Boer J 1955 *Physica* **21** 471–84
[26] Enting I G 1978 Generalised Mobius functions for rectangles on the square lattice *J. Phys. A: Math. Gen.* **11** 563–8
[27] Baake M, Grimm U, Repetowicz P and Joseph D 1998 Coordination sequences and critical points *Proc. 6th Int. Conf. on Quasicrystals (Tokyo, 1997)* ed S Takeuchi and T Fujiwara (Singapore: World Scientific) pp 124–7 (*Preprint* cond-mat/9809110)
[28] Dolbilin N P, Zinovev Yu M, Shtanko M A and Shtogrin M K 1998 The Kac combinatorial method *Russ. Math. Surv.* **53** 1346–47
[29] Repetowicz P, Grimm U and Schreiber M 2000 Planar quasiperiodic Ising models *Mat. Sci. Eng.* **294–296** 638–41
[30] Arisue H and Tabata K 1997 Low-temperature series for square lattice Potts model using the improved finite lattice method *J. Phys. A: Math.Gen.* **30** 3313–27
[31] Socolar J E S 1988 Simple octagonal and dodecagonal quasicrystals *Phys. Rev.* B **39** 10519–51
[32] Duneau M and Katz A 1985 Quasiperiodic patterns *Phys. Rev. Lett.* **54** 2688